Understanding the solubility of triamino-trinitrobenzene in hydrous tetramethylammonium fluoride: A first principles molecular dynamics simulation study

ARTICLE *in* PHYSICAL CHEMISTRY CHEMICAL PHYSICS · MARCH 2012

Impact Factor: 4.49 · DOI: 10.1039/c2cp22325b · Source: PubMed

4 AUTHORS, INCLUDING:

Bhabani S. Mallik
Indian Institute of Technology Hyderabad
23 PUBLICATIONS **204** CITATIONS

PCCP

Cite this: *Phys. Chem. Chem. Phys.*, 2012, **14**, 4884–4890

www.rsc.org/pccp

PAPER

Understanding the solubility of triamino-trinitrobenzene in hydrous tetramethylammonium fluoride: a first principles molecular dynamics simulation study

Bhabani S. Mallik,†[a] I-F. William Kuo,[b] Laurence E. Fried[b] and J. Ilja Siepmann*[a]

Received 16th July 2011, Accepted 9th February 2012
DOI: 10.1039/c2cp22325b

With the aim to understand the relatively high solubility of 1,3,5-triamino-2,4,6-trinitrobenzene (TATB), an important energetic material with a high degree of inter- and intra-molecular hydrogen bonding, in fluoride anion containing ionic liquids (ILs), first principles molecular dynamics simulations in the isobaric–isothermal ensemble were carried out for a system using hydrous tetramethylammonium fluoride as the prototypical solvent. Simulations initiated from both molecular TATB and its Meisenheimer complex (*i.e.*, a σ-complex of the fluoride and the electrophilic ring of TATB) yield a Zundel-type complex where a proton is shared between an amino group and an F^- ion, whereas the Meisenheimer complex is found to be only transiently stable. An analysis of the electronic structure probing the Wannier function centers supports the finding of a proton-sharing complex with a three-center four-electron like bond. The Zundel-type complex also yields an electronic absorption spectrum consistent with the experimentally observed color change. This study provides evidence that the remarkable solubility of otherwise hard-to-dissolve molecular crystals in ILs can be aided by chemical modification of the solute.

Introduction

1,3,5-Triamino-2,4,6-trinitrobenzene (TATB) is an important energetic material that is relatively insensitive to heat, impact, and shock,[1] but its very low solubility in common solvents[2] poses challenges for finding a formulation process that allows one to grow large and high-quality single crystals and thereby reduce the number of hot spots.[3] The crystalline form contains graphite-like sheets of TATB molecules that are connected through multiple hydrogen bonds,[4] and this extensive hydrogen-bond network is believed to be responsible for TATB's unusually large heat of sublimation and low solubility.

Ionic liquids (ILs) possess unique solubility characteristics,[5–7] for example chloride-containing ionic liquids are known to dissolve cellulose and other natural fibers.[8,9] Recently, relatively high TATB solubilities were observed in alkyl imidazolium ILs containing acetate (OAc^-) and fluoride anions but not for chloride anions.[10,11] However, a color change accompanied the solvation of TATB in both the F^- and OAc^- ILs and this indicates that a chemical modification of the solute may be at least partially responsible for the enhanced solubility. The formation of a Meisenheimer complex (*i.e.*, a σ-complex of the F^- or OAc^- and the electrophilic ring of TATB) or a hydrogen abstraction from the amino groups of TATB would be consistent with the observed color change.[10,11] Based on COSMO-RS calculations,[12] Maiti *et al.* suggested that cations with smaller alkyl ligands and compact cationic cores, such as tetramethyl ammonium (TMA), might be even better solvents for TATB than the alkyl imidazolium fluoride ILs.[10] In these COSMO-RS calculations, the IL was treated as an equimolar mixture of two components but the possibility of a chemical modification of the solute was not considered.

The aim of the present work is to investigate the solvation mechanism of TATB in the hydrous form of tetramethyl ammonium fluoride (TMAF). Since chemical events are likely contributing to the enhanced solubility of TATB in TMAF and the highly polar and heterogeneous solvation environment of the IL may play a role, we used a first principles molecular dynamics (FPMD) approach with explicit solvent for this computational study.

Simulation methods

The FPMD simulations were carried out with the Quickstep module of CP2K[13] where energies and forces are computed using the Gaussian plane wave method[14] with a dual basis set

[a] *Department of Chemistry and Department of Chemical Engineering and Materials Science and Chemical Theory Center, University of Minnesota, 207 Pleasant St. SE, Minneapolis, Minnesota 55455, USA. E-mail: siepmann@umn.edu*
[b] *Physical and Life Sciences Directorate, Lawrence Livermore National Laboratory, Livermore, California 94550, USA*
† Current address: Department of Chemistry, Indian Institute of Technology Hyderabad, Yeddumailaram, Andhra Pradesh 502205, India.

formalism of Gaussian-type orbitals for the real space components and plane waves for the expansion of the electronic density in reciprocal space to solve the self-consistent Kohn–Sham equations of density functional theory (DFT).[15] The DFT calculations used the Becke–Lee–Yang–Parr (BLYP) exchange/correlation functional,[16,17] norm-conserving Goedecker–Teter–Hutter pseudopotentials[18,19] for the core electrons, a double ζ plus polarization basis set (DZVP), and a density cutoff at 300 Ry for the auxiliary plane wave basis set. The electronic structure was optimized at every step (0.5 fs) of the trajectory (Born–Oppenheimer dynamics). The large system size studied here (see below) necessitates the use of a relatively small basis set and density cut-off. However, the combination of BLYP/DZVP has been shown to yield more accurate liquid-phase properties for water than BLYP with either the TZV2P or QZV3P basis set,[20] and a density cutoff at 300 Ry appears to yield more reasonable densities for neat and hydrous TMAF than a larger cutoff.[21] That is, for the specific system studied here the small basis set and charge density cutoff may compensate for deficiencies of the exchange/correlation functional.

The FPMD simulations were carried out in the isobaric–isothermal ensemble at a temperature of 400 K and a pressure of 1 atm using massive Nosé–Hoover chain thermostats (*i.e.*, a chain of 3 thermostats with a time constant of $\sim$33 fs for each degree of freedom)[22] and a barostat suggested by Mundy and co-workers.[23] A reference grid was used to avoid the large energy discontinuities that may be caused by changes in the number of reciprocal space vectors due to volume fluctuations.[23,24] This combination of thermostat and barostat was previously used in simulations of neat and hydrous TMAF and found to afford very good temperature control and significant volume changes during equilibration periods.[21]

Two independent runs (A and B) were carried out for a system consisting of one TATB molecule and 32 TMAF·H_2O formula units (696 atoms). This is a concentration similar to those found experimentally for alkyl imidazolium fluoride ILs and somewhat lower than the COSMO-RS prediction for the solubility in TMAF.[10] For run A, the system was pre-equilibrated using a Monte Carlo (MC) simulation in the isobaric–isothermal ensemble with TATB and TMAF described by the TraPPE force field[25,26] and water described by the SPC/E model,[27] followed by geometry optimization in CP2K before starting the FPMD trajectory that sampled the system for 45.5 ps. During the initial period of run A, there was no indication of the formation of a σ-complex. Thus, to explore the stability of the σ-complex, run B was set up using the configuration of run A at t = 5 ps but replacing the TATB molecule and nearest F^- ion by a σ-complex that was pre-optimized in the gas phase and consisted of the F^- ion bonded to a TATB ring carbon connected to an amino group. Again, geometry optimization was carried out for the solvated σ-complex before starting the FPMD trajectory. Run B was followed for only 21.6 ps because the σ-complex reverted back to a solvated structure with similar characteristics as found in run A. Although these runs are relatively long for a FPMD simulation of a 696-atom system, it cannot be ruled out that other forms of reactivity occurring at timescales inaccessible to FPMD simulations may also contribute to the enhanced solubility in fluoride ILs.

Results and discussion

Structural analysis

The focus of this work is on the TATB solute and its local solvation environment because the properties of the liquid phase of TMAF monohydrate without solute (and also of its anhydrous form) were described previously.[21] The trajectories of runs A and B were analyzed to find atom pairs that best characterize the solvation mechanism. The panels A and B of Fig. 1 depict the geometries of solvated TATB at the end of the MC and FPMD trajectories, respectively, of run A, and Fig. 2 shows the evolution of the characteristic pair distances for this FPMD trajectory. At the end of the MC pre-equilibration

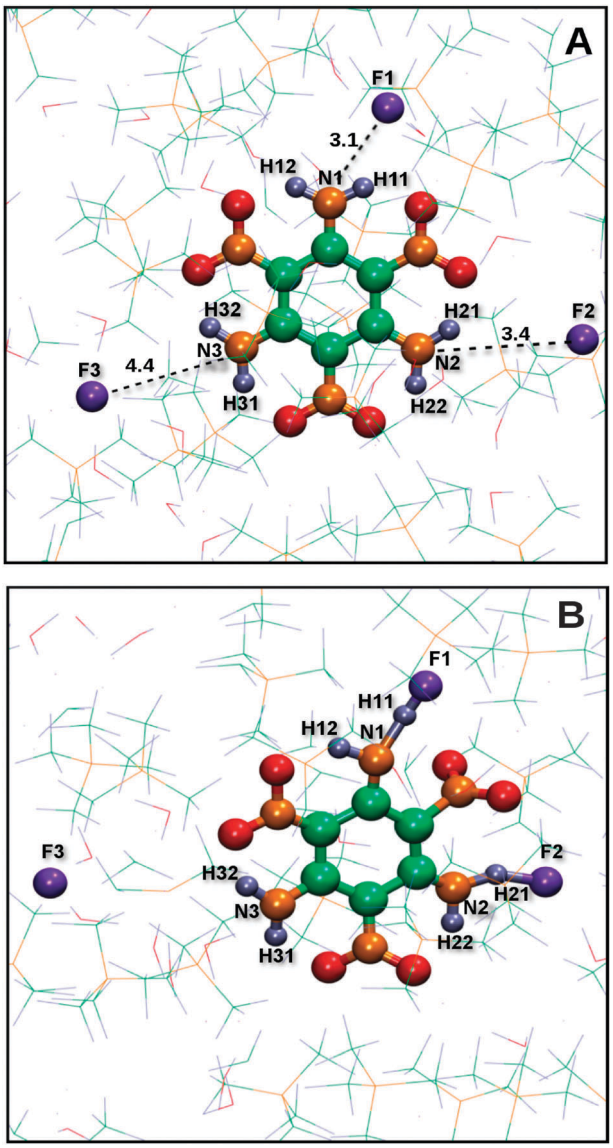

Fig. 1 The panels A and B depict the final configurations for the MC and FPMD trajectories, respectively, of run A. For better visual descriptions, the TATB molecule and the three F^- nearest to its amino groups are shown in ball and stick representation and the remainder of the system is shown in stick representation. C, N, O, H and F atoms are colored in green, orange, red, grey, and purple. The N–F distances are given in Å.

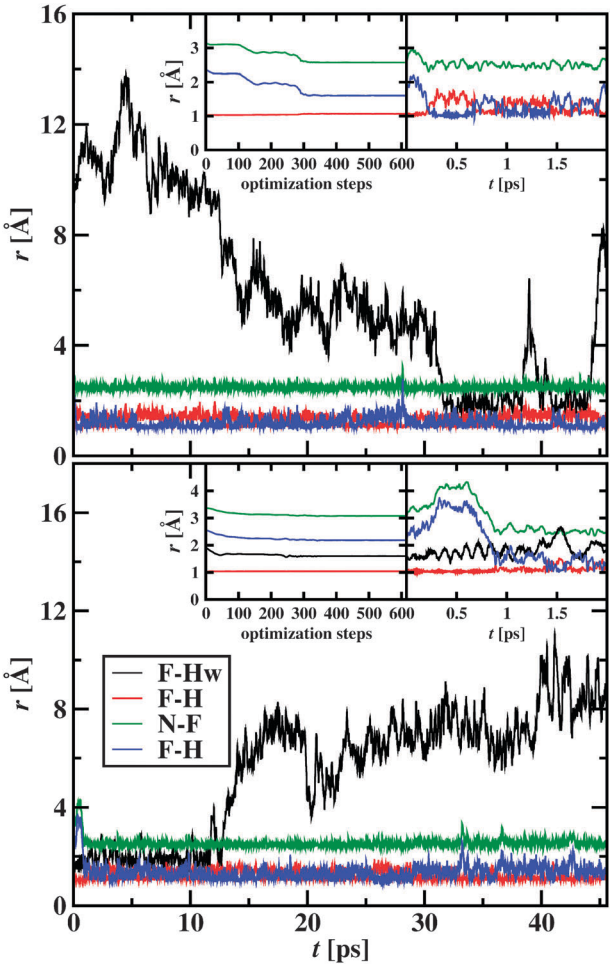

Fig. 2 The evolutions of the N–F, F–H, N–H, and F–H_w distances relevant for the formation of the partially deprotonated complex of TATB (run A) are depicted by green, blue, red, and black lines, respectively. H_w belongs to a water molecule that transiently forms a H-bond with one of the F^- ions. The insets depict these distances (left) during the geometry optimization of the structure taken from the MC trajectory and (right) during the first 2 ps of the FPMD trajectory. The upper and lower panels are for the amino groups labeled as 1 and 2 in Fig. 1.

period, the nearest F^- ions (labeled F1, F2 and F3) are found close to the three amino groups of TATB with N–F distances of 3.1, 3.4 and 4.4 Å, respectively, with the corresponding H–F distances being smaller by about 0.8 Å. During the CP2K geometry optimization, the N1–F1 and F1–H11 distances shorten significantly to values of 2.57 and 1.61 Å, respectively, and concomitantly the N1–H11 bond length of the amino group increases very slightly from 1.03 to 1.06 Å. The N2–F2 and F2–H21 distances also shorten but to a lesser extent during the geometry optimization, whereas the N3–F3 distance remains above 4 Å.

Thus, the optimization process led from a relatively weak (long) H-bond to a relatively strong (short) H-bond between the TATB amino groups (N1 and N2) and neighboring F^- ions (F1 and F2). This feature is also apparent from the radial distribution functions (RDFs) for each individual amino-group N atom with all the F^- ions (see Fig. 3). For the RDFs involving the N1 and N2 atoms, there is a very prominent

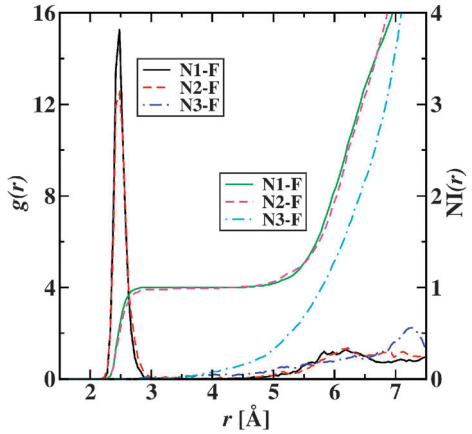

Fig. 3 Radial distribution functions and number integrals for individual amino-group N atoms with all the F^- ions from the FPMD trajectory of run A. The N1–F, N2–F, and N3–F RDFs are depicted by solid black, dashed red, and dash-dotted blue lines, respectively, and the corresponding NIs by solid green, dashed magenta, and dash-dotted cyan lines, respectively.

peak at r = 2.5 Å and the corresponding number integrals (NIs) reach unity at r = 2.8 Å for N1 and r = 4.1 Å for N2 (a NI of 0.97 is already reached at r = 2.8 Å), but this peak is absent for the N3 atom and the number integral reaches unity only at r = 5.8 Å. Thus, the remaining analysis emphasizes the two amino groups actively participating in the complexation of TATB.

During the initial part (t < 0.1 ps) of the FPMD trajectory, the N1–F1 and F1–H11 distances increase slightly, followed by a more substantial shortening (see insets of Fig. 2). At t = 0.2 ps, the F1–H11 and N1–H11 distances cross, *i.e.*, indicating a (partial) proton abstraction from the amino group to the F^- ion. However, at t = 0.7 ps, the process is reversed and the H atom is now again closer to the N atom than to the F^- ion. Such crossing events are also observed for the F2–H21 and N2–H21 distances at t = 1.4 and 1.7 ps. During the entire 45.5 ps trajectory, these crossings remain frequent but the N–F distances exhibit significantly smaller fluctuations, *i.e.*, an increase in the N–H distance is in most cases coupled with a concomitant decrease in the F–H distance and *vice versa*. These data clearly indicate the formation of a stable proton-sharing complex.

There are two other events involving the N1 amino group that are worth noting. Over the course of a few vibrational periods at $t \approx$ 28.1 ps, the F^- ion moves further away from the H atom than its usual oscillations and the F1–H11 and N1–F1 distances reach values of 2.8 and 3.3 Å, but this lengthening is very short-lived. At t = 31.5 ps, a water molecule moves in and forms an additional H-bond to the F^- ion of the proton-sharing complex. This H-bond is briefly broken at t = 39 ps, then remains present for another 3 ps, before it appears that the water molecule is diffusing away from the proton-sharing complex. For the N2 amino group, a H-bond to a water molecule is present from the outset, but this water molecule starts to move away at t = 12.5 ps. Thus, an additional H-bond with a water molecule appears to have only a rather small effect on the pair distances characteristic of the proton-sharing complex. This type of complex is somewhat analogous to the Zundel complex formed by sharing of a proton by two water molecules.[28,29]

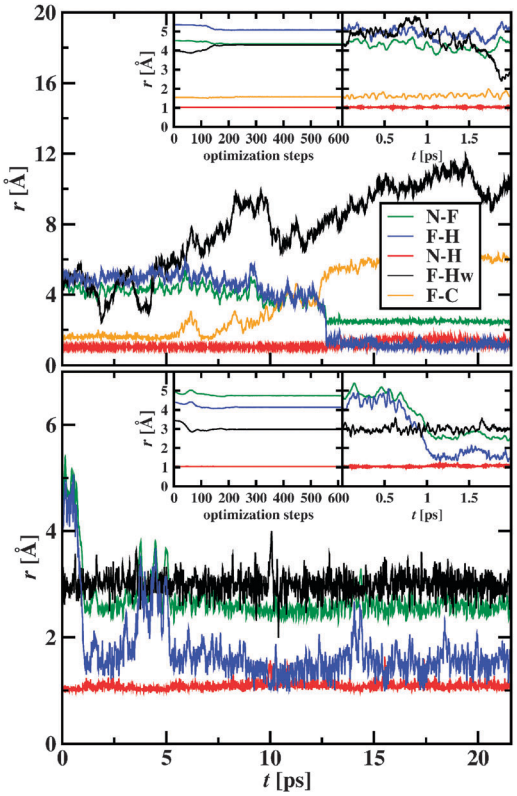

Fig. 4 The evolutions of the F–C, N–F, F–H, N–H, and F–H_w distances relevant for the breakage of the Meisenheimer complex and the formation of the partially deprotonated complex of TATB (run B) are depicted by orange, green, blue, red, and black lines, respectively. The upper and lower panels are for the amino groups N1 involved in the initial σ-complex and for another amino group N2. Other details as in Fig. 2.

The trajectory of run B was analyzed to probe the stability of the (pre-formed) σ-complex. The evolutions of different distances are depicted in Fig. 4. The upper panel indicates that the σ-complex is only transiently stable. This is evident from the F1–C distance that is close to 1.6 Å for the first 5.6 ps and again from t = 6.6 to 7.3 ps. This is followed by breakage of the F1–C bond and formation of molecular TATB. A water molecule is found to H-bond to the F atom at $t \approx 2$ and 4 ps and may be involved in facilitating the F1–C bond breakage. Over the next 5 ps, the F^- ion moves gradually away from the carbon atom and toward the N atom of another amino group (*i.e.*, not to the one connected to the carbon atom involved in the σ-complex). At t = 12.7 ps, a sudden jump occurs when the H11 atom of this other amino group N1 bridges to the F^- ion. At this point, the N1–F1 distance also shortens and the F1–C distance lengthens. For the remainder of run B, the F1–H11 and N1–H11 distances oscillate between 1 to 2 Å. During run B, another amino group N2 is also approached by an F^- ion at t = 1 ps and a partial deprotonation occurs. In this case, however, the N2–H21 distance is most of the time shorter than the F2–H21 distance and a water molecule stays in close proximity but does not H-bond to the F^- ion. The trajectory for run B clearly indicates that the Meisenheimer complex has only limited stability and that a proton-sharing complex similar to that found in run A is the preferred state

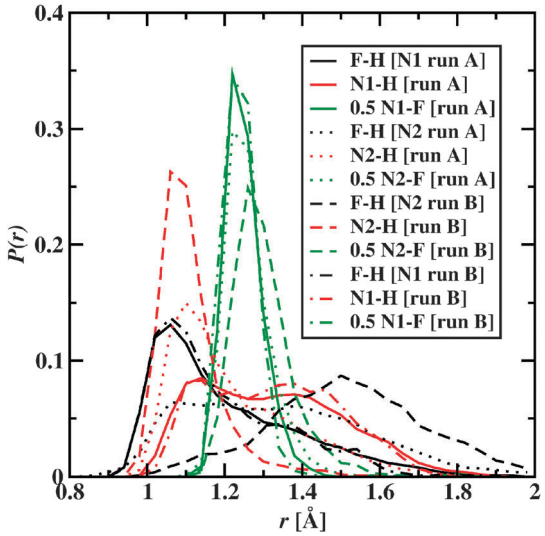

Fig. 5 Probability distributions for the F–H, N–H, and 0.5(F–N) distances are presented as black, red, and green lines, respectively. The distances involving the N1 and N2 atoms in run A are shown as solid and dotted lines, and those in run B (only for the final 8.9 ps) are shown as dash-dotted and dashed lines, respectively. The bin width is 0.04 Å.

for solvated TATB. Hoffman and Fontes[30] also reported decomposition of the Meisenheimer complex during the preparation of TATB crystals at T = 363 K, although different ILs were used in the experimental study.

The distributions of the N–F, N–H, and F–H distances of both the amino groups involved in the proton-sharing complex present throughout run A along with the corresponding distributions obtained during the last 8.9 ps for run B are provided in Fig. 5. For the amino group N1 of runs A and B, the N1–H11 distance distributions are bimodal with peaks at 1.14 and 1.38 Å, whereas the F1–H11 distances exhibit a single maximum at 1.06 Å with an extended tail toward larger distances. In both cases, the first peak is shifted by about 0.1 Å with respect to the corresponding sharp intramolecular distributions present for molecular ammonia and hydrogen fluoride,[31,32] but a significant part of the F–H distributions clearly occupies a region much shorter than a typical H-bond in the liquid phase of hydrogen fluoride.[32] The N2–H21 distance distributions for the second amino group (particularly for run B) do not exhibit the pronounced bimodal character and show a single peak at about 1.1 Å. Correspondingly, the F2–H21 distances are shifted to larger values with broad peaks centered at 1.25 and 1.5 Å for runs A and B, respectively. In contrast to the distances involving a H atom, the F–N distance distributions are much sharper with a peak at 2.44 Å (with the exception of N2–F2 for run B, where the peak is shifted slightly outward). Two-dimensional probability distributions for the N–H and F–H distances obtained from run B are shown in Fig. 6. The banana-shaped contours demonstrate the strong anti-correlation of the two distances involving the same proton. The peak towards the center of the banana and its ends-up orientation indicate that a proton-shared configuration is favored and results in somewhat shorter distances than a proton shuttling on a straight line between two endpoints.

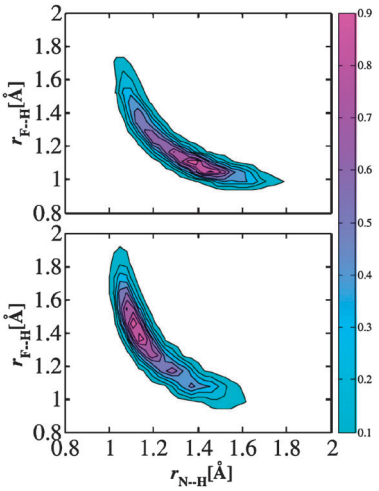

Fig. 6 Two-dimensional probability distributions for the F–H and N–H distances involving the N1 (top panel) and N2 (bottom panel) amino groups in run B.

Overall, these distributions further support the notion of a stable proton-sharing complex.

Using distance cut-offs at 1.12 and 1.02 Å for N–H and F–H covalent bonds, respectively, deduced from FPMD simulations of neat ammonia and hydrogen fluoride,[31,32] a H atom can be designated as being bound covalently to either N or F or as being shared (*i.e.*, not covalently bound) between both. (The probability that a H atom is bound covalently to both at the same time is negligible.) In run A, we find that a H-atom is shared with an F^- ion for both amino groups for 45% of the solvated TATB complexes, that one H-atom is bound to a N atom and the other is shared for 36% of the complexes, and that one H-atom is bound to an F atom irrespective of the state of the other H atom for 17% of the complexes. The corresponding probabilities for run B are 23, 59, and 11%, respectively. Thus, with a probability greater than 80% at least one of the amino groups is sharing its proton. Given the accessible run length and the sluggish dynamics of TMAF at 400 K,[21] a quantitative computation of the multi-dimensional (involving more than one amino group) free energy surface connecting the Meisenheimer and Zundel-type complexes is inaccessible with current computational resources. Similarly, it is currently not possible to evaluate the importance of nuclear quantum effects on the relative stability of the Meisenheimer and Zundel-type complexes. Path integral FPMD simulations of the hydrated excess proton and of triflic acid pentahydrate found only modest nuclear quantum effects on structural characteristics.[29,33]

Absorption spectra, energetics, and electronic properties

From the analysis of distance evolutions and distributions, it is clear that the proton-sharing (Zundel-type) complex is the most prevalent form of TATB in hydrous TMAF and may be responsible for the color change. The electronic absorption spectra for various TATB complexes taken from the FPMD simulations (see Fig. 7) but without any additional solvent components were calculated using INDO/CIS[34,35] as implemented

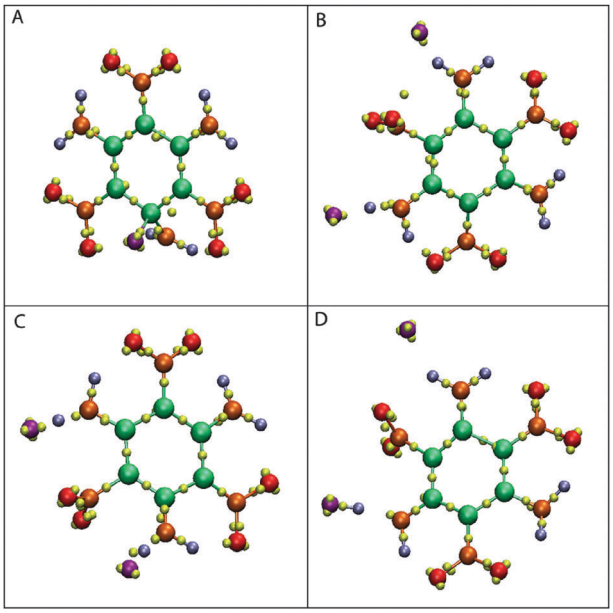

Fig. 7 Snapshots illustrating the Wannier function centers for various TATB complexes: (A) the Meisenheimer complex, (B) to (D) proton-sharing complexes with short (~1.0 Å), intermediate (~1.2 Å), and long (~1.7 Å) N–H distances as compared to F–H distances, respectively. The C, N, O, H, and F atoms are represented by green, orange, red, grey, and purple spheres, respectively, and the WFCs are represented by small yellow balls. Note that some of the WFCs are hidden behind the atoms.

in the ZINDO module of GAUSSIAN03.[36] This method is known to reproduce experimental absorption spectra with reasonable accuracy. The wavelength of the largest peak in the computed absorption spectra, λ_{max}, is 377 and 472 nm for molecular TATB and its Meisenheimer complex, respectively, as compared to values of 400, 425, and 440 nm for Zundel-type complexes with the H-atoms being shared with an F^- ion for both amino groups, with one H-atom being shared and the other bound to an amino group, and with one H-atom bound to an F atom and the other bound to an amino group, respectively. The change in the chemistry (σ bond for the Meisenheimer complex and partial abstraction of the proton for the Zundel-type complex) leads to additional delocalization (spreading) of the highest occupied molecular orbital and, hence, a shift of the absorption maximum to a larger wavelength particularly for the Meisenheimer complex. Experimentally, $\lambda_{max} \approx 360$ and 420 nm are found for TATB solvated in dimethyl sulfoxide and in $BuMim^+F^-$, respectively.[10,11] This comparison lends further support to the notion that the solvated species is the proton-sharing complex and not the Meisenheimer complex.

Due to the large system size, the FPMD simulations were carried out with a relatively small basis set. To probe the energetics of the four clusters shown in Fig. 7, we have computed the binding energies for the *unsolvated* clusters with the DZVP and TZV2P basis sets without and with the Grimme D3 dispersive correction.[37] For all four combinations of basis set/dispersive correction, the Zundel-type complex (C) with the intermediate N–H distance yields the most favorable binding energy, followed by the complex (D) with the long N–H distance, then complex (B) with the short N–H distance,

and the Meisenheimer complex (A) has the least favorable binding energy. The difference between cluster (C) and the Meisenheimer complex (A) falls in the range from 100 to 120 kJ mol^{-1}, but it should be noted that the Meisenheimer complex contains only one F^- ion, whereas the Zundel-type complexes contain two ions. For all four clusters, the combination of D3–DZVP yields the most favorable binding energy, followed in order by DZVP, D3–TZV2P, and TZV2P. Of course, these binding energies can only provide a rough guide to the free energy landscape of complexes solvated by explicit TATB.

To provide further insight into the electronic structure of the complexes observed in the FPMD simulations, the Wannier function centers (WFCs)[38] were determined. The location of these WFCs provides a means of assessing the existence of a bond and its type between atoms. Fig. 7 depicts the WFCs for three proton-sharing complexes with various N–H and F–H distances and for the Meisenheimer complex. For the latter, one WFC is found on the C–F bond but it is displaced toward the F atom. For all of the proton-sharing complexes, a WFC is located between N and H atoms and another WFC between F and H atoms. For the proton-sharing complex with $r_{N-H} \approx r_{F-H}$, the two WFCs are found $\sim$0.8 Å away from the proton toward the N and F atoms and the WFC–H–WFC angle is $\sim$160°, a structure that closely resembles the Zundel complex of protonated water molecules.[29,39] There are minor changes in the WFC geometry of the structures depending on the location of the proton. For example, for structures with $r_{N-H} \approx$ 1.0, $\approx$ 1.2, and $\approx$ 1.7 Å, the calculated average angles between the N-WFC and F-WFC vectors are 130°, 160°, and 150° based on 5 structures for each category. Overall, the location of the WFCs also supports the formation of a three-center four-electron like bond[40] between N, H, and F atoms.

Conclusions

First principles molecular dynamics simulations in the isobaric–isothermal ensemble exploring the solvation of TATB in hydrous TMAF indicate that the unusually high solubility[10] and color change[10,11] are due to the formation of proton-sharing complexes where the N and H atoms of two amino groups and two F^- ions are involved in two three-center four-electron bonds, whereas the Meisenheimer complex with a σ bond between one of the ring C atoms and an F^- ion is found to possess only limited stability.[30] The nature of the proton-sharing complex is elucidated from various distance distributions and the location of Wannier function centers. Absorption spectra for the proton-sharing complex are also more consistent with experimentally observed color changes than the spectrum for the Meisenheimer complex. Overall, the outcome of our FPMD simulations (chemical modification, color change, and instability of the Meisenheimer complex) correlates well with recent experimental studies on solvation of TATB in ILs,[10,11,30] and taken together show that formation of a Zundel-type complex is responsible for the unusually high solubility of TATB in F^- ion containing ILs. Complexation with amino groups or other suitable functional groups by F^- ion containing ILs may be a general mechanism for solubility enhancements.

Acknowledgements

Financial support from the Department of Energy (contract DE-AC52-07NA27344 to Lawrence Livermore National Laboratory, Laboratory Directed Research and Development Program Project 06-SI-005, subcontract B559898) and the National Science Foundation (CBET-0756641) is gratefully acknowledged. Computer resources were provided by the Minnesota Supercomputing Institute and the Lawrence Livermore National Laboratory.

References

1 C. M. Tarver, J. W. Kury and R. Breithaupt, Detonation Waves in Triaminotrinitrobenzene, *J. Appl. Phys.*, 1997, **82**, 3771–3782.
2 W. Selig, Estimation of the Solubility of 1,3,5-triamino-2,4,6-trinitrobenzene (TATB) in Various Solvents, *LLNL Technical Report*, 1977, UC-ID 17412.
3 C. M. Tarver, S. Chidester and A. L. Nichols, Critical Conditions for Impact- and Shock-induced Hot Spots in Solid Explosives, *J. Phys. Chem.*, 1996, **100**, 5794–5799.
4 H. H. Cady and A. C. Larson, The Crystal Structure of 1,3,5-Triamino-2,4,6-Trinitrobenzene, *Acta Crystallogr.*, 1965, **18**, 485–496.
5 T. Welton, Room-Temperature Ionic Liquids. Solvents for Synthesis and Catalysis, *Chem. Rev.*, 1999, **99**, 2071–2084.
6 J. S. Wilkes, A Short History of Ionic Liquids from Molten Salts to Neoteric Solvents, *Green Chem.*, 2002, **4**, 73–80.
7 R. D. Rogers and K. R. Seddon, Ionic Liquids-Solvents of the Future?, *Science*, 2003, **302**, 792–793.
8 R. P. Swatloski, S. K. Spear, J. D. Holbrey and R. D. Rogers, Dissolution of Cellose with Ionic Liquids, *J. Am. Chem. Soc.*, 2002, **124**, 4974–4975.
9 D. M. Phillips, L. F. Drummy, D. G. Conrady, D. M. Fox, R. R. Naik, M. O. Stone, P. C. Trulove, H. C. De Long and R. A. Mantz, Dissolution and Regeneration of Bombyx mori Silk Fibroin using Ionic Liquids, *J. Am. Chem. Soc.*, 2004, **126**, 14350–14351.
10 A. Maiti, P. F. Pagoria, A. E. Gash, T. Y. Han, C. A. Orme, R. H. Gee and L. E. Fried, Solvent Screening for a Hard-to-Dissolve Molecular Crystal, *Phys. Chem. Chem. Phys.*, 2008, **10**, 5050–5056.
11 T. Y.-J. Han, P. F. Pagoria, A. E. Gash, A. Maiti, C. A. Orme, A. R. Mitchell and L. E. Fried, The Solubility and Recrystallization of 1,3,5-Triamino-2,4,6-Trinitrobenzene in a 3-Ethyl-1-Methylimidazolium Acetate-DMSO Co-solvent System, *New. J. Chem.*, 2009, **33**, 50–56.
12 A. Klamt, *COSMO-RS: From Quantum Chemistry to Fluid Phase Thermodynamics and Drug Design*, Elsevier, Amsterdam, 2005.
13 J. VandeVondele, M. Krack, F. Mohamed, M. Parrinello, T. Chassaing and J. Hutter, QUICKSTEP: Fast and Accurate Density Functional Calculations Using a Mixed Gaussian and Plane Waves Approach, *Comput. Phys. Commun.*, 2005, **167**, 103–128.
14 G. Lippert, J. Hutter and M. Parrinello, A Hybrid Gaussian and Plane Wave Density Functional Scheme, *Mol. Phys.*, 1997, **92**, 477–488.
15 W. Kohn and L. J. Sham, Self-consistent Equations Including Exchange and Correlation Effects, *Phys. Rev. A: At., Mol., Opt. Phys.*, 1965, **140**, A1133–A1138.
16 A. D. Becke, Density-functional Exchange-Energy Approximation with Correct Asymptotic Behavior, *Phys. Rev. A*, 1988, **38**, 3098–3100.
17 C. T. Lee, W. T. Yang and R. G. Parr, Development of the Colle-Salvetti Correlation-Energy Formula into a Functional of the Energy Density, *Phys. Rev. B: Condens. Matter*, 1988, **37**, 785–789.
18 S. Goedecker, M. Teter and J. Hutter, Separable Dual-space Gaussian Pseudopotentials, *Phys. Rev. B: Condens. Matter*, 1996, **54**, 1703–1710.
19 C. Hartwigsen, S. Goedecker and J. Hutter, Relativistic Separable Dual-space Gaussian Pseudopotentials from H to Rn, *Phys. Rev. B: Condens. Matter*, 1998, **58**, 3641–3662.
20 M. J. McGrath, J. I. Siepmann, I. W. Kuo and C. J. Mundy, Vapor-liquid Equilibria of Water from First Principles: Comparison of Density Functionals and Basis Sets, *Mol. Phys.*, 2006, **106**, 3619–3626.

21 B. S. Mallik and J. I. Siepmann, Thermodynamic, Structural and Transport Properties of Tetramethyl Ammonium Fluoride: First Principles Molecular Dynamics Simulations of an Unusual Ionic Liquid, *J. Phys. Chem. B*, 2010, **114**, 12577–12584.

22 G. J. Martyna, M. L. Klein and M. E. Tuckerman, Nose-Hoover Chains: The Canonical Ensemble *via* Continuous Dynamics, *J. Chem. Phys.*, 1992, **97**, 2635–2643.

23 J. Schmidt, J. VandeVondele, I.-F. W. Kuo, D. Sebastiani, J. I. Siepmann, J. Hutter and C. J. Mundy, Isobaric–Isothermal Molecular Dynamics Simulations Utilizing Density Functional Theory: An Assessment of the Structure and Density of Water at Near-Ambient Conditions, *J. Phys. Chem. B*, 2009, **113**, 11959–11964.

24 M. J. McGrath, J. I. Siepmann, I. W. Kuo, C. J. Mundy, J. VandeVondele, J. Hutter, F. Mohamed and M. Krack, Isobaric–Isothermal Monte Carlo Simulations from First Principles: Application to Liquid Water at Ambient Conditions, *ChemPhysChem*, 2005, **6**, 1894–1901.

25 N. Rai, D. Bhatt, J. I. Siepmann and L. E. Fried, Monte Carlo Simulations of 1,3,5-Triamino-2,4,6-Trinitrobenzene (TATB): Pressure and Temperature Effects for the Solid Phase and Vapor-Liquid Phase Equilibria, *J. Chem. Phys.*, 2008, **129**, 194510.

26 C. D. Wick, J. Stubbs, N. Rai and J. I. Siepmann, Transferable Potentials for Phase Equilibria. 7. United-Atom Description for Nitrogen, Amines, Amides, Nitriles, Pyridine and Pyrimidine, *J. Phys. Chem. B*, 2005, **109**, 18974–18982.

27 H. J. C. Berendsen, J. R. Grigera and T. P. Straatsma, The Missing Term in Effective Pair Potentials, *J. Phys. Chem.*, 1987, **91**, 6269–6271.

28 G. Zundel and H. Metzger, Energiebänder der tunnelnden Überschuss-Protonen in flüssigen Säuren-Eine IR-spektroskopische Untersuchung der Natur der Gruppierungen $H_5O_2^+$, *Z. Phys. Chem.*, 1968, **58**, 225–245.

29 D. Marx, M. E. Tuckerman, J. Hutter and M. Parrinello, The nature of the hydrated excess proton in water, *Nature*, 1999, **397**, 601–604.

30 D. M. Hoffman and A. T. Fontes, Density Distribution in TATB Prepared by Various Methods, *Propellants, Explos., Pyrotech.*, 2010, **35**, 15–23.

31 M. Diraison, G. J. Martyna and M. E. Tuckerman, Simulation Studies of Liquid Ammonia by Classical *ab initio*, Classical and Path-integral Molecular Dynamics, *J. Chem. Phys.*, 1999, **111**, 1096–1103.

32 M. Kreitmeir, H. Bertagnolli, J. J. Mortensen and M. Parrinello, *Ab initio* Molecular Dynamics Simulation of Hydrogen Fluoride at Several Thermodynamic States, *J. Chem. Phys.*, 2003, **118**, 3639–3645.

33 R. L. Hayes, S. J. Paddison and M. E. Tuckerman, Proton Transport in Triflic Acid Pentahydrate Studied *via Ab initio* Path Integral Molecular Dynamics, *J. Phys. Chem. A*, 2011, **115**, 6112–6124.

34 J. E. Ridley and M. C. Zerner, Triplet-States *via* Intermediate Neglect of Differential Overlap- Benzene, Pyridine and Diazines, *Theor. Chim. Acta*, 1976, **42**, 223–236.

35 W. P. Anderson, W. D. Edwards and M. C. Zerner, Calculated Spectra of Hydrated Ions of the First Transition-metal Series, *Inorg. Chem.*, 1986, **25**, 2728–2732.

36 M. J. Frisch, *et al.*, *Gaussian 03, Revision C.02*, Gaussian, Inc., Wallingford, CT, 2004.

37 S. Grimme, Semiempirical GGA-type density functional constructed with a long-range dispersion correction, *J. Comput. Chem.*, 2006, **27**, 1787–1799.

38 N. Marzari and D. Vanderbilt, Maximally Localized Generalized Wannier Functions for Composite Energy Bands, *Phys. Rev. B: Condens. Matter*, 1997, **56**, 12847–12865.

39 V. Buch, A. Dubrovskiy, F. Mohamed, M. Parrinello, J. Sadlej, A. D. Hammerich and J. P. Devlin, HCl Hydrates as Model Systems for Protonated Water, *J. Phys. Chem. A*, 2008, **112**, 2144–2161.

40 G. Pimentel, The Bonding of Trihalide and Bifluoride Ions by the Molecular Orbital Method, *J. Chem. Phys.*, 1951, **19**, 446–448.